Environmental Chemistry and Ecotoxicology 3 (2021) 241–248

Contents lists available at ScienceDirect

Environmental Chemistry and Ecotoxicology

journal homepage: www.keaipublishing.com/en/journals/environmental-chemistry-and-ecotoxicology/

Structure, morphology and electrochemical properties of $SrTiO_3$ perovskite: Photocatalytic and supercapacitor applications

V.V. Deshmukh [a,*], C.R. Ravikumar [b], M.R. Anil Kumar [b], Suresh Ghotekar [c], A. Naveen Kumar [b], A.A. Jahagirdar [d], H.C. Ananda Murthy [e,*]

[a] Department of Physics, Shri Shivaji Science College, Amravati, Maharashtra 444602, India
[b] Research Centre, Department of Science, East West Institute of Technology, Bangalore 560091, India
[c] Department of Chemistry, Smt. Devkiba Mohansinhji Chauhan College of Commerce and Science, University of Mumbai, Silvassa 396 230, Dadra and Nagar Haveli (UT), India
[d] Department of Chemistry, Ambedkar Institute of Technology, Bangalore 560056, India
[e] Department of Applied Chemistry, School of Applied Natural Science, Adama Science and Technology University, PO Box 1888, Adama, Ethiopia

ARTICLE INFO

Article history:
Received 12 June 2021
Received in revised form 19 July 2021
Accepted 19 July 2021
Available online 22 July 2021

Keywords:
$SrTiO_3$ NPs
Sol-gel
Photocatalyst
Cyclic voltammetry
Supercapacitance

ABSTRACT

In order to explore an alternative photocatalyst for environmental remediation, we report the sol-gel process for the synthesis of strontium titanate ($SrTiO_3$) nanoparticles (STNPs). The as-synthesized STNPs were found to poses cubic perovskite-type crystal structure with an average crystallite size of 22 nm were well-characterized by X-ray diffraction (XRD). The agglomerated and cubic like morphologies were identified by using scanning electron microscopy (SEM). The elemental analysis by energy dispersive X-Ray spectroscopy (EDAX) confirmed the composition of STNPs. The synthesized nanoparticles were further characterized by Fourier transform infrared (FTIR) analysis. STNPs displayed good photocatalytic degradation activity for malachite green (MG) and rhodamine blue (Rh–B) dye pollutants under UV light irradiation in the time duration of 120 min. Furthermore, cyclic voltammetric studies revealed that the STNP electrode, because of its increased surface area, produced maximal specific capacitance of 208.47 Fg^{-1} at 1 mA/cm^2 with a high cycle stability of 1500 cycles. The superior supercapacitance behaviour of $SrTiO_3$ electrode materials strengthens its stance to be developed as a highly promising material for energy related applications. In addition, STNPs can serve as better materials for the environmental remediation of pollutant dyes.

1. Introduction

The challenging issue of energy harvesting and storage requires immediate attention. In order to meet the increasing demand of energy consumption, high performance materials with appreciable energy conversion efficiency at minimal energy loss are being extensively researched in the recent years. Supercapacitors are one such class of materials which are popular for their enhanced power density over batteries and superior energy density than conventional capacitors [1]. The recent studies have revealed that the transition metal oxides with perovskite structure are better candidate for delivering high electrochemical performance over a large potential window [2–4]. Perovskites are metal oxides with ABO_3structurewith peculiar charge ordering [5] that has led to their multifunctional and diversified applications such as in solar cells [6], photo-degradation of dyes [7], Li-ion batteries [8], supercapacitors [9] and electrochemical sensors [10]. Among many perovskite structured metal oxides, $SrTiO_3$ was found to exhibit wide range of applications in microelectronics owing to its outstanding properties such as charge storage capacity, insulating property, optical transparency and chemical stability [11–13]. The sol-gel process gives various advantages over conventional synthetic strategies. It provides homogeneous blending of reactants on the molecular stage and may be adopted to govern shape, morphology and particle length of the ensuing product. In this work, we have synthesized perovskite type $SrTiO_3$ nanoparticles (STNPs) by sol–gel method calcined at 550 °C and their applications as photocatalysts and electro-active materials have been investigated.

According to literature $SrTiO_3$ with perovskite structure which exhibited a pseudo capacitive behaviour of the nanoparticles. $SrTiO_3$ is a characteristic perovskite-type oxide whose physical properties powerfully depend on its chemical composition, structure, shape, size, and crystallinity. Strontium titanate is one of the most significant multifunctional perovskites used

* Corresponding authors.
E-mail addresses: vaishalideshmukh27@gmail.com (V.V. Deshmukh), ananda.murthy@astu.edu.et (H.C.A. Murthy).

Production and hosting by Elsevier on behalf of KeAi

http://dx.doi.org/10.1016/j.enceco.2021.07.001

in the manufacture of electronic gadgets, photoanode for quantum dot–sensitized solar cells, and electroceramics [14,15].

Furthermore, for instance, $SrTiO_3$ NPs have applications in dielectrics, thermistors, multilayer capacitors, electro-optical appliances, electromechanical devices, and field effect transistors [16]. $SrTiO_3$ is an n-type semiconductor with cubic perovskite structure, and it has an indirect band gap that varies from 3.2 to 3.4 eV, although some recent work shows that there is an increase in band gap to 3.77 eV causing a photon emission in the blue green region of the spectrum [17,18].

In the present work, we have synthesized STNPs NPs using sol-gel method with a short calcination time and studied their supercapacitor and photocatalytic studies. In the sol-gel method, preparations of macro-crystalline, structured particles are reduced into nano-crystalline structures, but the original reliability of the material is retained. Furthermore, the electrode was assembled using PVDF/KCl electrolyte reveals maximum specific capacitance of 208.47 Fg^{-1} at 1 mA/cm^2 with a high cycle stability of 1500 cycles. This is originating equivalent to many reports. Therefore, STNPs can be suggested as a potential electrode for supercapacitors and acts as a good photocatalyst for dye decolarization.

2. Materials and methods

2.1. Materials

Strontium nitrate $Sr(NO_3)_2$, Titanium(IV) n-butoxide ($C_{16}H_{36}O_4Ti$), Citric acid ($C_6H_8O_7$), Ethanol (CH_3CH_2OH), Polyvinylidene difluoride (PVDF) and *N*-methyl-2-pyrrolidone (C_5H_9NO) were obtained from Sigma Aldrich company.

2.2. Synthesis of $SrTiO_3$ nanoparticles (STNPs)

The starting chemicals used for the synthesis of STNPs, are strontium nitrate $Sr(NO_3)_2$, Titanium (IV) n-butoxide ($C_{16}H_{36}O_4Ti$) and citric acid. The stoichiometric amount of strontium nitrate and titanium n-butoxide were dissolved in a minimum amount of ethanol and followed by the addition of citric acid in the molar ratio 1:1 to chelate the cations in the solution. Further, the complex solution was treated with ethanol to regulate the viscosity and thereby manage the velocity of the metal ions, which results in the gelation of reaction mixture. The resulting mixture was subjected to evaporation on a magnetic stirrer at a temperature of 80 °C to get a gel, which was then poured into a pressure bomb for annealing in a tubular furnace at 120 °C for 12 h followed by an initial calcination at 350 °C for 4 h and further calcination at 550 °C for 6 h.

2.3. Characterization of STNPs

The product was characterized by Panalytical X-ray diffractometer (X'pert pro MPD) fitted with Cu Kα sealed tube (λ = 1.5406 Å) in a 2θ scan range from 20 to 80° with a step size of 0.016°. The morphological features were examined by field-emission scanning electron microscope (FESEM Zeiss Ultra plus). The Energy Dispersive X-ray (EDAX) spectrometer coupled FESEM was used to analyse the sample composition. Fourier transform infrared spectra of the powdered sample were recorded using a Perkin Elmer FTIR ATR spectrometer. The electrochemical performance of the STNPs was investigated on a CHI608E instrument for cyclic voltammetry (CV). The chrono-potentiometry (CP) tests were conducted by using a three-electrode cell with STNP as a working electrode, platinum foil (counter electrode) and Ag/AgCl (reference electrode).

2.4. Electrochemical characterization

The STNPs working electrode was prepared by mixing 80 wt% of the synthesized STNPs and 20 wt% of binder polyvinylidene difluoride (PVDF) in *N*-methyl-2-pyrrolidone (NMP). This mixture was uniformly dispersed on nickel mesh and dried at room temperature for 24 h. The alternating current (AC) impedance measurement was carried out at open circuit potential in the frequency range between 0.01 Hz and 1 M Hz with alternating current amplitude of 5 mV. All electrochemical measurements were carried out in 1 M aqueous KCl solution as electrolyte. The specific capacitance in Fg^{-1} was calculated from the CV curve as [19–22],

$$C = \frac{S}{2mK\Delta V} \quad (1)$$

where,

m is the weight of the material loaded on the electrode,

ΔV is the voltage window, and k is the scan rate under the cyclic voltammogram.

The specific capacitance of STNP was deduced from the galvanostatic charge-discharge (GCD) curve using the eq. (2) [23],

$$C = \frac{i}{-\frac{\Delta V}{\Delta t} \times m} = \frac{i}{-slope \times m} \quad (2)$$

where i is the current applied and $\Delta V/\Delta t$ is the slope of the discharge curve after IR drop.

3. Results and discussion

3.1. XRD analysis

The diffraction pattern of the STNPs calcined at 550 °C is as shown in Fig. 1. The sample is highly crystalline as depicted by the presence of sharp peaks which can be well indexed to (100,110,111,200,211,220,310) planes of the cubic perovskite $SrTiO_3$ structure. This result is in compliance with the standard data with JCPDS card no. 35–0734 and 79–0176. In addition, the XRD pattern revealed negligible and minor impurity peaks. The average crystallite size of STNPs was calculated by using the Debye-Scherrers formula (3) [24],

$$D = \frac{K\lambda}{\beta\cos\theta} \quad (3)$$

where D is the average crystallite size, k is a constant (with a value of 0.89), λ = 1.5405 Å (Cu Kα radiation), β is the full width at half maximum of the

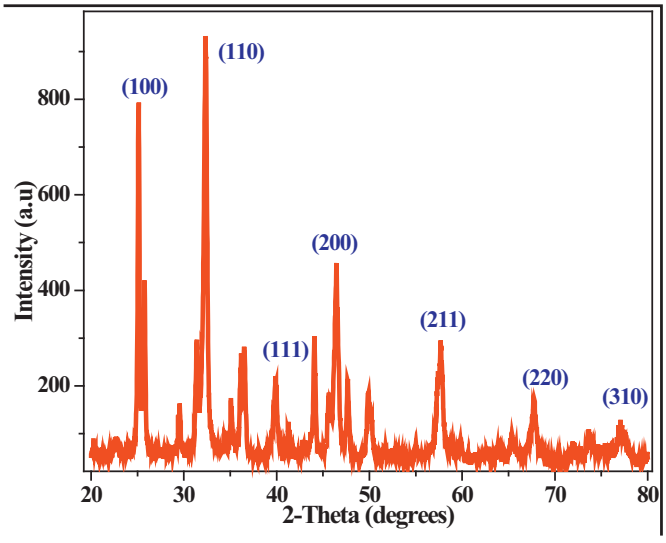

Fig. 1. XRD pattern of $SrTiO_3$ nanoparticles (STNPs).

Table 1
XRD parameters of $SrTiO_3$ nanoparticles calcined at 550 °C.

2θ (deg)	Interplanar spacing (*d*) (A°)	FWHM (deg)	Crystallite size (nm)	*hkl*	Lattice constant (*a*) (A°)
32.397	2.7612	0.386	22.4	110	3.9048
39.926	2.2562	0.442	20.0	111	3.1907
46.384	1.9560	0.495	18.2	200	2.7661
57.683	1.5968	0.250	37.4	211	2.2581
67.630	1.3842	0.510	19.7	220	1.9575
77.014	1.2372	0.850	12.5	310	1.7496

diffraction peaks and θ is the Bragg's angle. The lattice parameter (a) was calculated from the diffraction planes using the formula (4) [25],

$$a = \frac{d}{\sqrt{h^2 + k^2 + l^2}} \quad (4)$$

where d is the interplanar distance and h, k, l are Miller indices.

The crystallite sizes of STNPs deduced by Scherrer's equation are listed in Table 1. The average crystallite size of 22.4 nm was obtained based on the full width at half maximum intensity of the (110) peak. The calculated lattice parameter for the same peak was found to be 3.9048 Å which is in good agreement with the literature values confirming the cubic perovskite crystal structure of $SrTiO_3$ [26,27].

3.2. FTIR analysis

Infrared spectral analysis is a powerful tool to identify the metal-oxygen bonding in the final product post calcination. FT-IR spectra are recorded for the percentage transmittance against the wave number in the range of 4000–400 cm^{-1} as shown in Fig. 2. The IR peak at 1444.86 cm^{-1} can be associated with hydroxyl group from the adsorbed water. The absorption peaks at around 856 cm^{-1} and 437.91 cm^{-1} can be attributed to the presence of Ti–O_6 octahedron stretching and Ti–O bending vibrations respectively [28]. The prominent peak at 543.09 cm^{-1} is a characteristic peak of $SrTiO_3$ corresponding to Sr-Ti-O stretching vibration [29]. The absence of impurity peaks in the FTIR spectra clearly confirms the formation of pure $SrTiO_3$ nanostructures.

3.3. SEM analysis

Fig. 3 (a) and (b) shows the morphology of the STNPs at different magnifications. The image reveals the formation of well-organized cubic structures of the products which is similar to that of sintered ceramics obtained by solid state reaction. The average particle size was found to be ~40 nm. Morphology shows porous surface (can't make out porous nature) which can be beneficial for ion diffusion and can show good electrochemical response. Further, the dominance of Sr, Ti and O elements in the EDAX is a significant evidence of $SrTiO_3$ formation (Fig. 3c). The low intensity peak for carbon shows traces of impurities.

3.4. Photocatalytic study

3.4.1. Preparation of dyes solution for 20 ppm

0.1 g dye dissolved in to 100 ml distilled water and 5 ml of this solution diluted in 250 ml Standard flask. 250 ml of prepared dye solutions were taken into circular glass reactor along with 0.06 g STNPs catalyst. This mixture is stirred and is irradiated by a 400 W Hg lamp. 5 ml of sample solution was withdrawn after 15 min of time intervals successively.

3.4.2. Photocatalytic measurements

The photocatalytic experiments were performed for degradation of Malachite Green (MG) and Rhodamine Blue (Rh–B) dyes at a constant concentration of 20 ppm. For this, 60 mg of STNPS photocatalyst was mixed with 250 ml aqueous solution of MG and Rh–B dyes separately. The solutions were taken in a circular glass reactor (176.6 cm^2 surface area) and irradiated less than 125 W mercury vapour lamp acting as source of UV light. The UV light irradiation was carried out by directly focusing into the reaction solution from a vertical distance of 23 cm in the open air condition [30,31]. The solution was continuously stirred throughout the 2 h long experiment. After every 15 min of time interval, 5 ml of the sample solution was withdrawn and absorbance was measured. As mentioned in Fig. 4, the photocatalytic efficiency of STNP on the photodegradation of the cationic MG dye (λ_{max} 483 nm) and Rh–B dye (λ_{max} 501 nm) were investigated. The degree of adsorption (Q) was deduced by using the following eq. (5),

$$Q = \frac{(C_0 - C)V}{W} \quad (5)$$

where, C_0 and C are dye solution concentrations before and after adsorption, V is volume of the reaction mixture and W is mass of the catalyst [32].

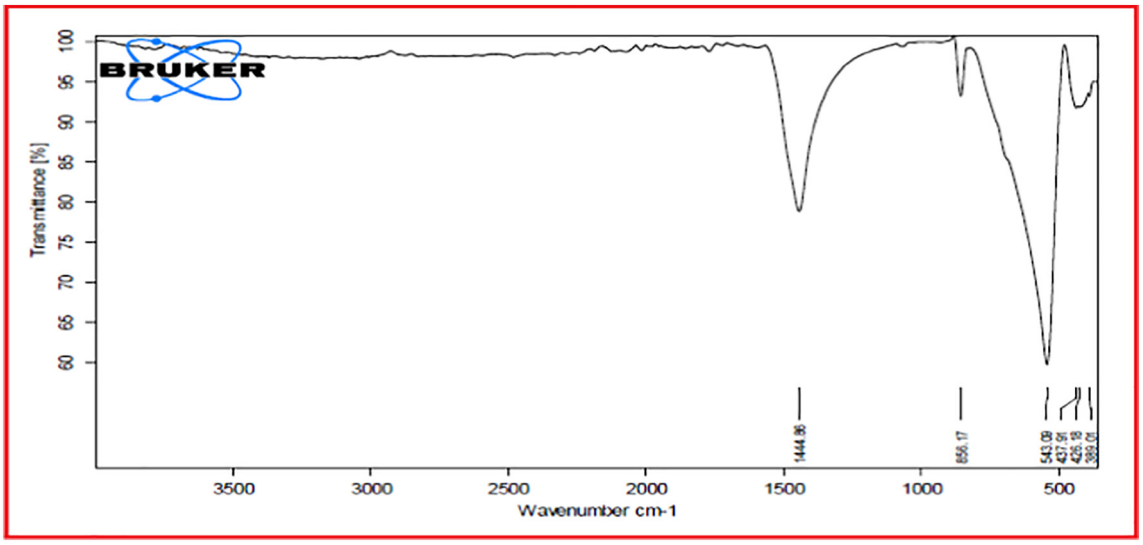

Fig. 2. FTIR spectrum of STNPs.

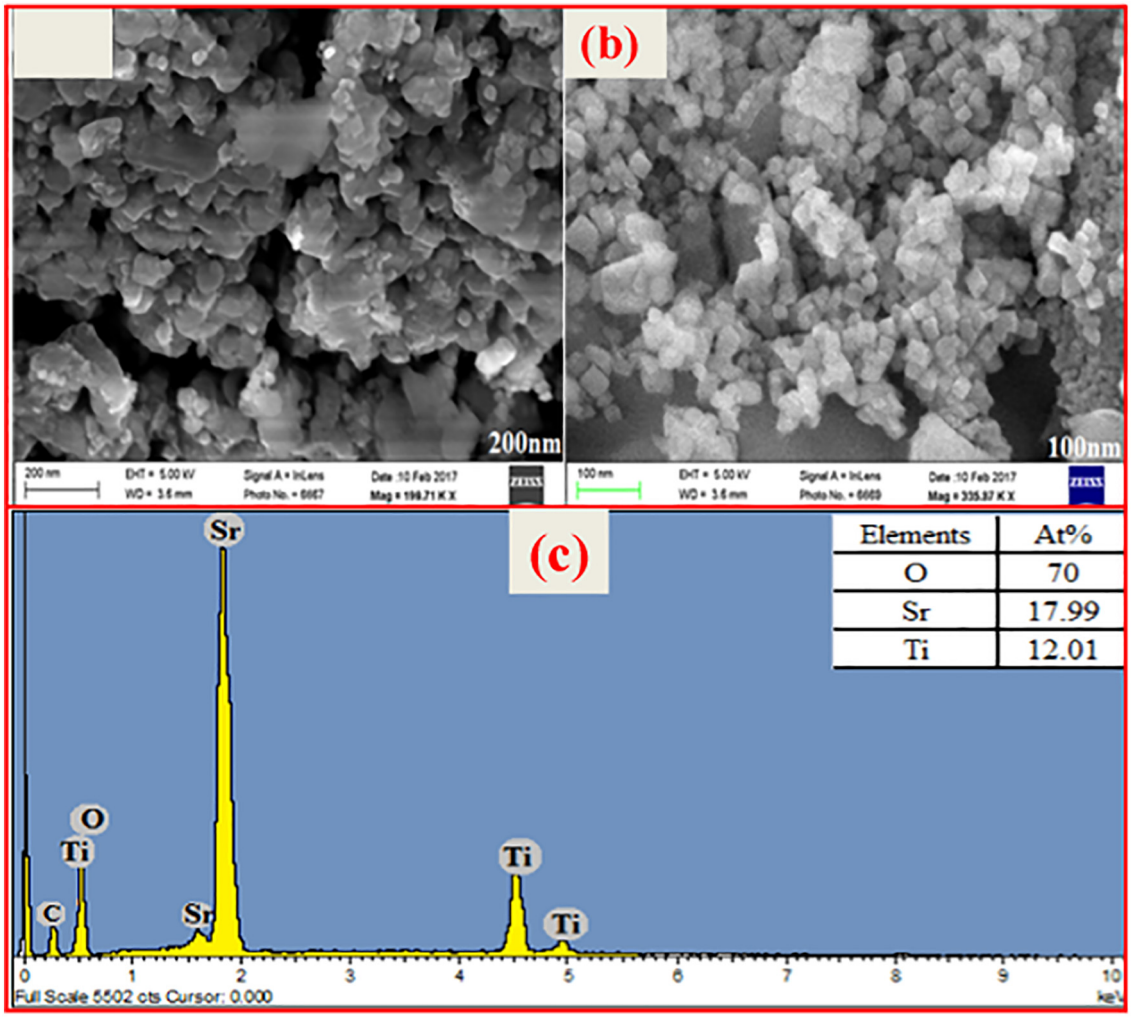

Fig. 3. FESEM images of STNPs at magnification (a) 199.71 KX (b) 335.87 KX c) EDAX spectrum of STNPs and elements present in the compound with their concentrations.

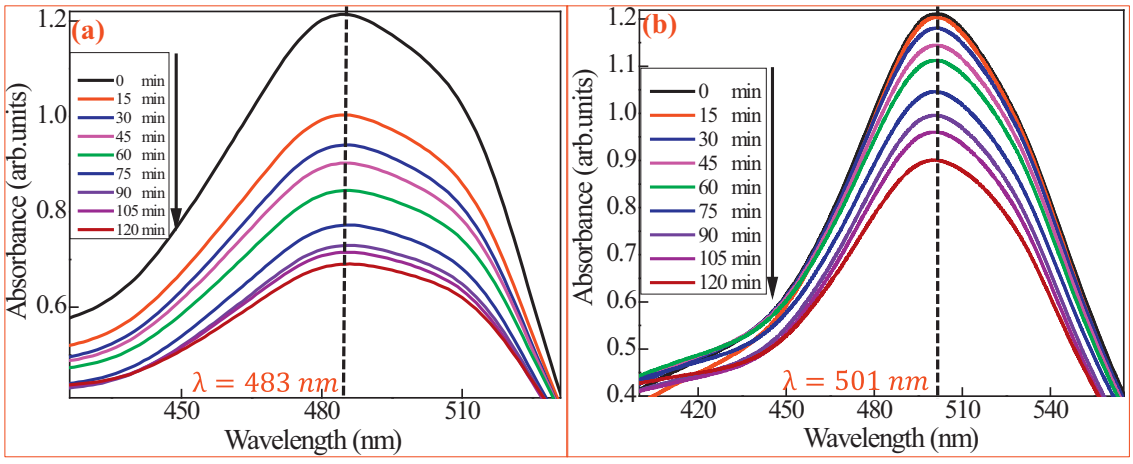

Fig. 4. Absorbance spectra of MG and RhB with STNP photocatalyst.

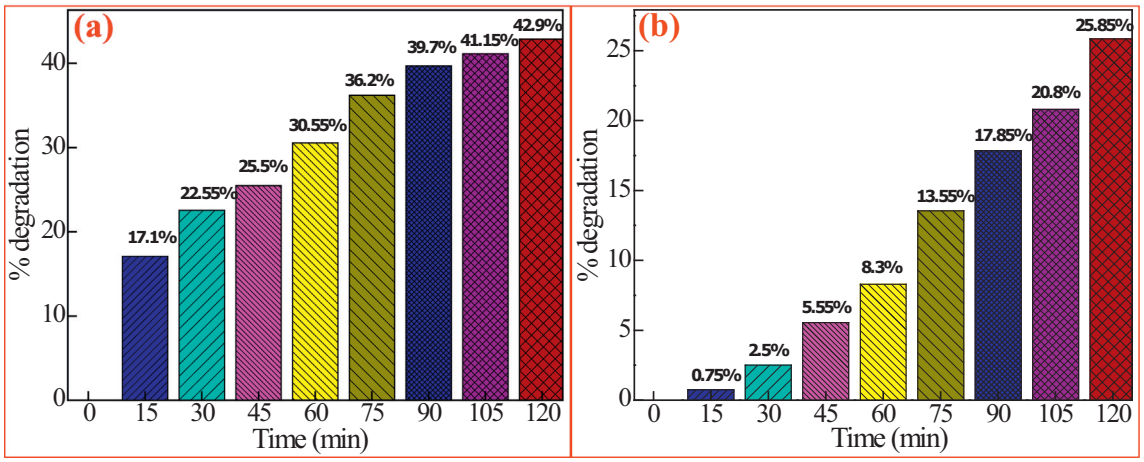

Fig. 5. Plot of % degradation of MG and RhB dyes under UV light.

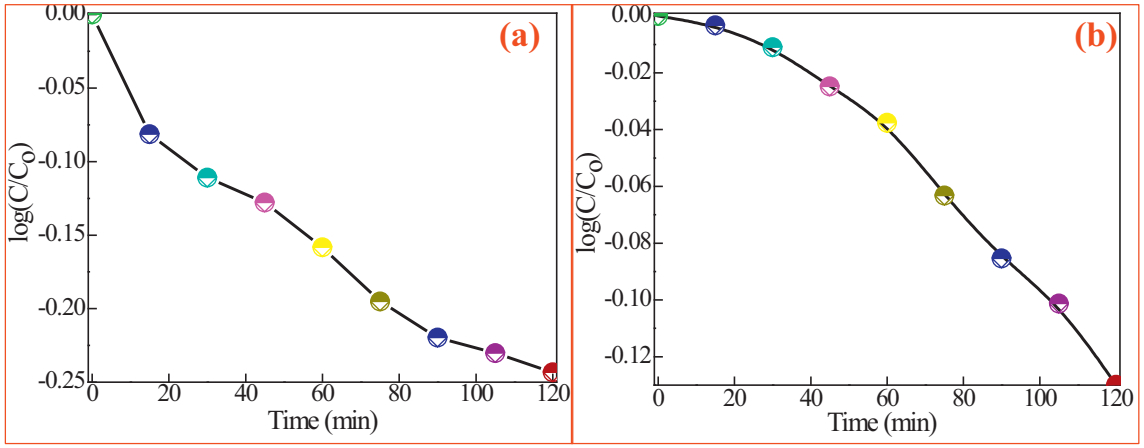

Fig. 6. Plot of logC/Co for the degradation of MG and RhB dyes under UV light.

Also, degradation percentage (*%D*) was calculated from the eq. (6) [33,34] and the values have been plotted in Fig. 5.

$$(\%D) = \frac{C_o - C}{C_o \times 100} \tag{6}$$

It was observed that in the initial 15 min, MG undergoes degradation of 17.1%. However, the degradation rate improves with time achieving 42.9% degradation at the end of 120 min. Similarly, the Rh–B dye could achieve a degradation of 25.85% at the end of 120 min.

The kinetics of the photodegradation reaction was studied by using the following Eq. [35].

$$\frac{logC}{C_0} = -kt \tag{7}$$

where, k is a first order rate constant and t is time. A plot of log (C/C_0) vs. time revealed a linear relationship of log C/C_0 and t confirming the first order kinetics (Fig. 6). The slope k was calculated as 0.005574 $min^{-1}$and 0.001486 min^{-1} for MG and Rh–B respectively are as presented in Table S1 and Table S2 [36]. The results are encouraging and signal the adequacy of $SrTiO_3$ in degradation of hazardous dyes like MG and Rh–B and may also be useful for the removal of secondary pollutants. The structural features of MG and Rh–B dyes are presented in Table S3.

3.4.3. Mechanism of photocatalytic degradation

When STNPs were subjected to UV light with energy higher than the band gap energy, the formation of positively charged holes (h^+) takes place in the valence band (VB) by transfer of electrons ($e-$) to the conduction band (CB) [37]. Due the benefit of small size, the photogenerated electrons have easy access to the STNPs catalyst wherein they easily reduce molecular oxygen to reactive radical species (O_2^-). Concurrently, the holes created in the VB converts the water molecules to reactive hydroxyl radicals (OH^-). The active radical species so generated along with the photogenerated holes accelerate the degradation of the adsorbed dye molecules [38]. Additionally, to complete photodegradation process, active photo excited electrons and holes also degrade the dye molecules. Detailed schematic diagram representing the mechanism of photo assisted decolorization of textile dye is shown in Fig. S1. The main steps involved in reaction process of photocatalytic degradation under UV light irradiation can be given as follows:

$$SrTiO_3 + h\nu \rightarrow e^- + h^+ \tag{8}$$

$$O_2 + e^- \rightarrow O^*_2 \tag{9}$$

$$OH + h^+ \rightarrow OH^* \tag{10}$$

$$OH^- + O_2{}^- + \text{Dyes} \rightarrow \text{Decomposed products} \tag{11}$$

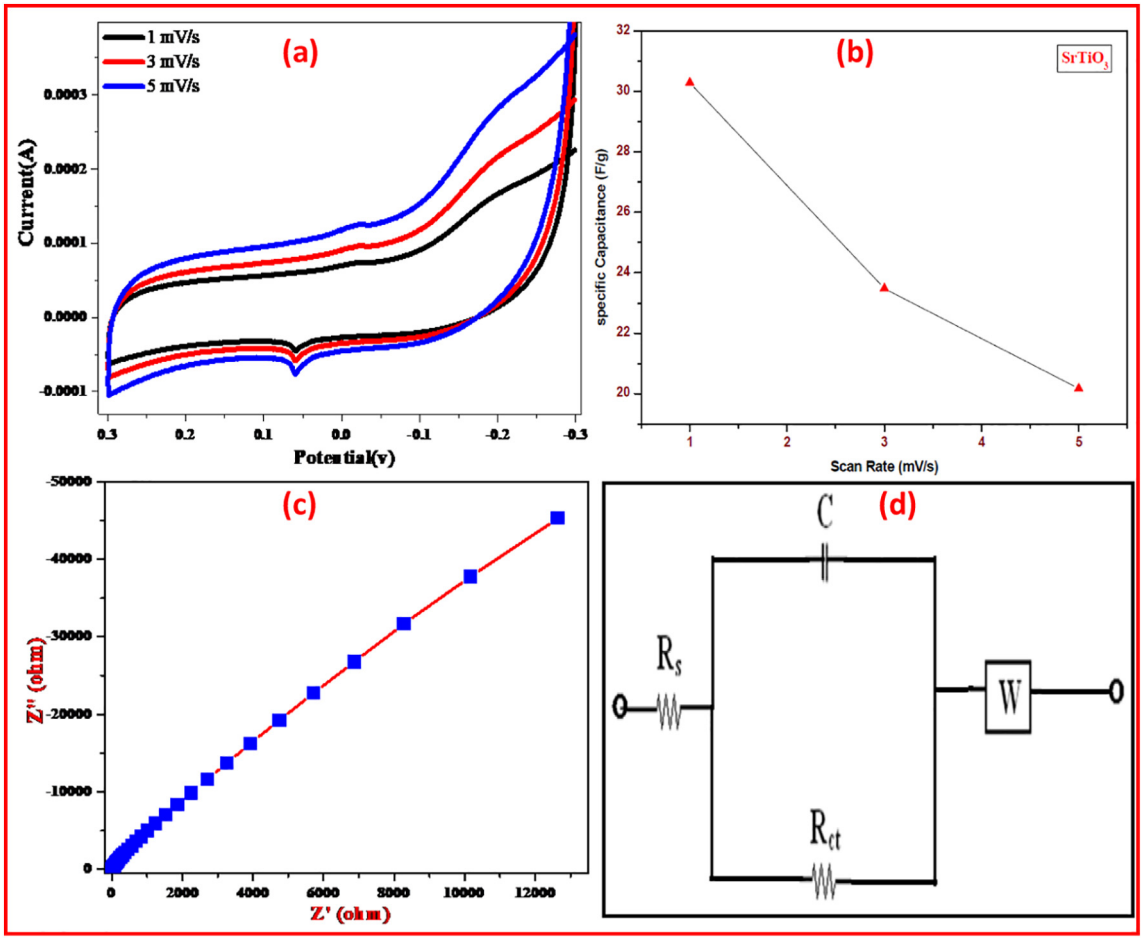

Fig. 7. (a) Cyclic voltammograms of STNP(b) Scan rate vs specific capacitance profile for STNP. (c) EIS spectra of STNP conducted in 1 M KCl. (d) Equivalent circuit of EIS spectra.

3.5. Evaluation of electrochemical properties

3.5.1. Cyclic voltammetry studies of STNP electrode

Cyclic voltammetry (CV) measurements were performed for STNPs based electrode on nickel mesh as electrochemical electrode using a three-electrode cell in 1 M KCl aqueous solution. A potential window of −0.3 to 0.3 V versus Ag/AgCl electrode used was maintained at various scan rates. Fig. 7 (a) shows the CV curves for STNP working electrode recorded at the scan rate of 1 mV/s, 3 mV/s and 5 mV/s respectively. At a low scan rate of 1 mV/s the CV curve displays a rectangle shape which is a sign of charge-discharge reversibility taking place at the electrode/electrolyte interface [39–41]. As the scan rate increases, the area under the "rectangle" increases. Also, very weak redox peak signals are observed for the samples at all the scan rates. From the CV curves, specific capacitance values were calculated using the eq. 1. The average specific capacitance obtained for STNP electrode was 202.86 Fg^{-1}, at the scan rate of 1mVs^{-1}.

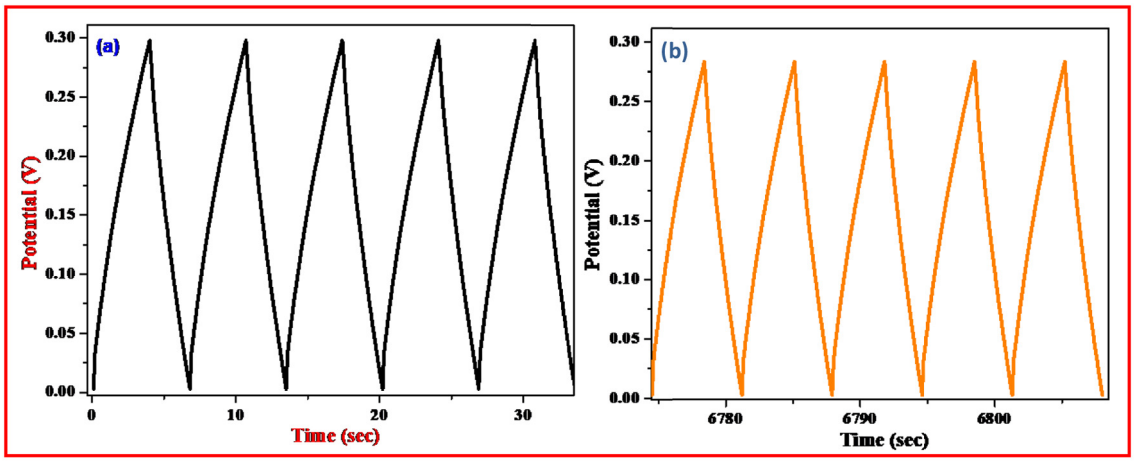

Fig. 8. Galvanostatic Charge-Discharge curve of STNPs (a) First five cycles and (b) 1500th cycles.

Fig. 7(b) shows that as the scan rate increases value of specific capacitance decreases. However, throughout the study, STNPs were found to be electrochemically stable and active. We believe that by tailoring the size and shape of STNPs, it is possible to achieve electrodes with better super capacitive characteristics.

3.5.2. EIS analysis of STNP electrode

The electron impedance spectroscopy (EIS) analysis was carried out to study the electrical conduction and ion transfer reactions occurring on the electrode surface. In the present work, the EIS data were recorded in of 0.1 Hz to 1 MHz frequency range by applying 5 mV amplitude AC voltage. The Nyquist plot of the STNP electrode is shown in Fig. 7(c) and the corresponding equivalent circuit for curve fitment is shown in Fig. 7(d). As can be seen from Fig. 7(c), the semi-circle in the high frequency region of the Nyquist plot is too small to be detected while the plot gets extended as a straight, slope line in the low frequency region [42]. The depressed semicircle in the plot is an indication of a very small charge transfer resistance occurring at the electrode/electrolyte interface. The linear extended imaginary part in the low frequency region is a representation of the capacitive nature of an electrode and in the present case, it can be clearly seen that the plot is equivalent to a straight line similar to an ideal capacitor [43]. The estimated equivalent series resistance (ESR) value for the $SrTiO_3$ nanocubes is 3.613 Ω. The value indicates good electrochemical performance by $SrTiO_3$ nanocubes.

3.5.3. Galvanostatic charge–discharge studies of STNP electrode

The galvanostatic charge–discharge characteristics of the STNP electrode was explored using chrono-potentiometry between 0 and 0.3 V potential window, at a current density of 5 $Ag^{-1}$and in 1 M KCl electrolyte (Fig. 8). The triangular shape of the curve indicates good charge–discharge reversibility and electrode stability. The discharge specific capacitance of 208.47 Fg^{-1} was obtained (eq. 2) for $SrTiO_3$ electrode, which is approximately same as that obtained from CV curve, further highlighting the excellent electrochemical capability of STNPs electrode. Further, the electrode also reported a good cycling stability (~90%) after 1500 cycles.

Fig. 9 reveals the electrochemical impedance spectra of STNP electrode before and after charge-discharge subjected to 1500 cycles. It is observed that even at the end of 1500 charge-discharge cycles, no drastic change in resistance of the electrode was observed as confirmed by AC impedance graph [44]. Thus, STNP electrode is believed to retain high stability even after charge-discharge behaviour. The prepared STNP electrode showed a minimum charge-transfer resistance which is possibly due to its high conductivity as supported by electrochemical impedance studies. The results

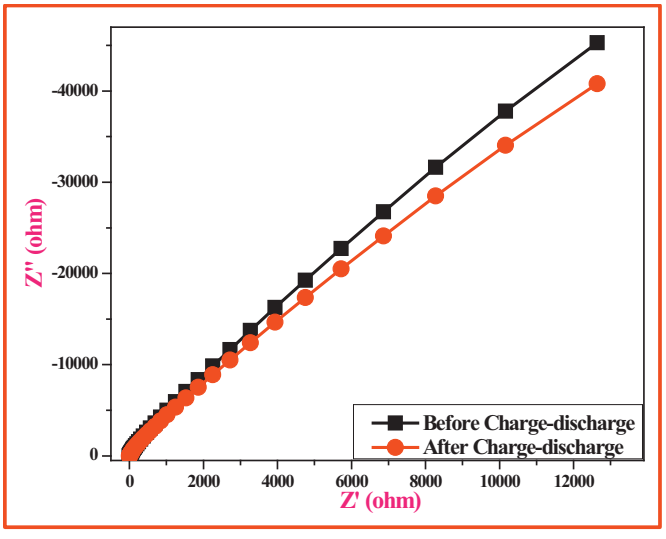

Fig. 9. EIS spectra of STNPelectrode before and after charge-discharge of 1500 cycles.

clearly show that STNP can act efficiently as better material for supercapacitor applications.

4. Conclusion

$SrTiO_3$ nanoparticles (STNPs) were successfully synthesized by using sol-gel method. $SrTiO_3$ exhibited cubic perovskite ABO_3 type crystal structure with an average crystalline domain of 22 nm. The absorption peaks occur in IR spectra further confirm the formation of pure STNPs nanoparticles. Microstructure through SEM revealed cubic shaped nature of the nanocrystals. The photocatalytic studies carried out for MG and Rh–B dye pollutants under UV light showed highest % D for MG of 42.9% at the end of 120 min. Electrochemical characteristics of STNPs electrode were investigated by CV, EIS and GCD studies. $SrTiO_3$ electrode showed maximum specific capacitance of 208.47 Fg^{-1}at the scan rate of 1mVs^{-1}. The high conductivity and high cycling stability (1500 cycles) of the material are the added characteristic features required for an ideal electrochemical supercapacitor. Also, STNPs low cost and non-hazardous nature offers greater advantages over other transition-metal oxides than those currently being used for this purpose.

Declaration of Competing Interest

On behalf of all authors, the corresponding authors states that there is no conflict of interest.

Acknowledgement

The authors are grateful to Nanotechnology Research lab, Department of Chemistry, Shri Shivaji Science College, Amravati for providing research facilities. The authors also wish to thank VGST, Govt. of Karnataka, India (Nos VGST/CISEE/2014-15/282 and VGST/K-FIST-L1/2014-15/GRD-360) for extending their support to carry out this research work.

Appendix A. Supplementary data

Supplementary data to this article can be found online at https://doi.org/10.1016/j.enceco.2021.07.001.

References

[1] B.E. Conway, Electrochemical Supercapacitors, Kluwer-Academic, 1999.
[2] C.D. Lokhande, T.P. Gujar, V.R. Shinde, R.S. Mane, S.H. Han, Electrochemical supercapacitor application of pervoskite thin films, Electrochem. Commun. 9 (2007) 1805–1809.
[3] N. Padmanathan, S. Selladurai, R.K. Mani, C. O'Dwyer, K.M. Razeeb, NiO hybrid nanoarchitecture-based pseudocapacitor in organic electrolyte with high rate capability and cycle life, Ionics 21 (2015) 2623–2631.
[4] Y. Cao, B. Lin, Y. Sun, H. Yang, X. Zhang, Sr-doped lanthanum Nickelate Nanofibers for high energy density Supercapacitors, Electrochim. Acta 174 (2015) 41–50.
[5] N.C. Bristowe, J. Varignon, D. Fontaine, E. Bousquet, P. Ghosez, Ferromagnetism induced by entangled charge and orbital orderings in ferroelectric titanate perovskites, Nat. Commun. 6 (2015) 1–8.
[6] A. Bera, K. Wu, A. Shaikh, E. Alarousu, O.F. Mohammed, T. Wu, Perovskite oxide $SrTiO_3$ as an efficient Electron transporter for hybrid Perovskite solar cells, J. Phys. Chem. C 118 (2014) 28494–28501.
[7] S. Tonda, S. Kumar, O. Anjaneyulu, V. Shanke, Synthesis of Cr and La-codoped SrTiO3 nanoparticles for enhanced photocatalytic performance under sunlight irradiation, Phys. Chem. Chem. Phys. 16 (2014) 23819–23828.
[8] Z. Shen, Z. Wang, B. Luo, L. Li, $BaTiO_3$–$BiYbO_3$ perovskite materials for energy storage applications, J. Mater. Chem. 3 (2015) 18146–18153.
[9] D.K. Hwang, S. Kim, J.H. Lee, I.S. Hwang, D. Kim, Phase evolution of perovskite $LaNiO_3$ nanofibers for supercapacitor application and p-type gas sensing properties of LaOCl–NiO composite nanofibers, J. Matere. Chem. 21 (2011) 1959–1965.
[10] B. Wang, B. Gu, Y. Ding, Y. Chu, Z. Zhang, B. Ba, Q. Zhang, X. Li, A novel route to prepare $LaNiO_3$ perovskite-type oxide nanofibers by electrospinning for glucose and hydrogen peroxide sensing, Analyst 138 (2013) 362–367.
[11] K. Karthick, S.R. Ede, U. Nithiyanantham, S. Kundu, Low temperature synthesis of $SrTiO_3$ nano assemblies on DNA scaffolds and their applications in dye-sensitized solar cells and supercapacitors, New J. Chem. 41 (2017) 3473–3486.
[12] C. Chen, Q. Dai, C. Miao, Strontium titanate nanoparticles as the photoanode for CdS quantum dot sensitized solar cells, RSC Adv. 5 (2015) 4844–4852.

[13] C.N. George, J.K. Thomas, R. Jose, Synthesis and characterization of nanocrystalline strontium titanate through a modified combustion method and its sintering and dielectric properties, J. Alloys Compd. 486 (2009) 711–715.
[14] M.A. Farrukh, K.M. Butt, K.K. Chong, W.S. Chang, Photoluminescence emission behavior on the reduced band gap of Fe doping in CeO_2-SiO_2 nanocomposite and photophysical properties, J. Saudi Chem. Soc. 23 (2019) 561–575.
[15] M. Sharma, S. Sen, G. Jagannath, M. Ghosh, S. Pitale, G. Vinay, S.C. Gadkari "Tuneable blue-green emission from ZnS(Ag) nanostructures grown by hydrothermal synthesis", J. Mater. Res. 33 (2018) 3963–3970.
[16] K. Naidu, S.T. Sofi, V. Reddy, M. Maddaiah, P. Reddy, T. Subbarao, Structural, dielectric and electrical properties of La_2O_3doped $SrTiO_3$ceramics, J. Aust. Ceram. Soc. 51 (2015) 94–102.
[17] J. Lin, J. Cheng, P. Li, W. Chen, H. Huang, Study on SrTiO3 film for the application of power devices, Superlattice. Microst. 130 (2019) 168–174.
[18] H. Gao, H. Yang, S. Wang, Hydrothermal synthesis, growth mechanism, optical properties and photocatalytic activity of cubic $SrTiO_3$ particles for the degradation of cationic and anionic dyes, Optik 175 (2018) 237–249.
[19] M.A. Shilpa Amulya, H.P. Nagaswarupa, M.R. Anil Kumar, C.R. Ravikumar, K.B. Kusuma, Sonochemical synthesis of MnFe2O4 nanoparticles and their electrochemical and photocatalytic properties, J. Phys. Chem. Solids 148 (2021) 109661.
[20] M.A. Shilpa Amulya, H.P. Nagaswarupa, M.R. Anil Kumar, C.R. Ravikumar, S.C. Prashantha, K.B. Kusuma, Sonochemical synthesis of $NiFe_2O_4$ nanoparticles: characterization and their photocatalytic and electrochemical applications, Appl. Surf. Sci. Adv. 1 (2020) 100023.
[21] V.V. Deshmukh, H.P. Nagaswarupa, C.R. Ravikumar, M.R. Anil Kumar, T.R. Shashi Shekhar, H.C. Ananda Murthy, Lanthanum doped strontium Titanate nanomaterial for Photocatalytic and Supercapacitor applications, Asian J. Chem. 32 (2020) (2013-2020).
[22] N.B. Arun Kumar, B. Mahendra, J. Sirajudeeen, M.R. Anil Kumar, H.P. Nagaswarupa, C.R. Ravikumar, B. Umesh, Green mediated synthesis of MgO Nano-flakes and its electro-chemical applications, Mater. Today Proc. 5 (2018) 22275–22282.
[23] C. Pratapkumar, S.C. Prashantha, H. Nagabhushana, M.R. Anilkumar, C.R. Ravikumar, H.P. Nagaswarupa, D.M. Jnaneshwara, White light emitting magnesium aluminate nanophosphor: Near ultraviolet excited photoluminescence, photometric characteristics and its UV photocatalytic activity, J. Alloys Compd. 728 (2017) 1124–1138 Elsevier.
[24] K.C. Babu Naidu, T. Sofi Sarmash, M. Maddaiah, A. Gurusampath Kumar, D. Jhansi Rani, V. Sharon Samyuktha, L. Obulapathi, T. Subbarao, Structural and electrical properties of pbO – doped $SrTiO_3$ ceramics, J. Ovonic Res. 11 (2015) 79–84.
[25] K.C. Babu Naidu, T. Sofi Sarmash, T. Subbarao, Preparation and characterization of nano $SrTiO_3$ ceramics, Int. J. Phys. Res. 4 (2014) 31–36.
[26] S. Sahani, T. Roy, Y. Sharma, Studies on fast and green biodiesel production from an indigenous nonedible Indian feedstock using single phase strontium titanate catalyst, Energy Convers. Manag. 203 (2020) 112180.
[27] Q.A. Zhu, J.G. Xu, S. Xiang, L.X. Chen, Z.G. Tan, Preparation of $SrTiO_3$ nanoparticles by the combination of solid phase grinding and low temperature calcining, Mater. Lett. 65 (5) (2011) 873–875 15.
[28] Q.R. Deng, X.H. Xia, M.L. Guo, Y. Gao, G. Shao, Mn-doped TiO_2Nanopowders with remarkable visible light Photocatalytic activity, Mater. Lett. 65 (2011) 2051–2054.
[29] M.R. Anil Kumar, C.R. Ravikumar, H.P. Nagaswarupa, B. Purshotam, Bedasa Abdisa Gonfa, H.C. Ananda Murthy, FedluKedir Sabir, Samson Tadesse, Evaluation of bi- functional applications of ZnO nanoparticles prepared by green and chemical methods, J. Env Chem Eng. 7 (2019) 103468.
[30] M.R. Anil Kumar, H.P. Nagaswarupa, C.R. Ravikumar, S.C. Prashantha, H. Nagabhushana, Aarti S. Bhatt, Green engineered nano MgO and ZnO doped with Sm^{3+}: synthesis and a comparison study on their characterization, PC activity and electrochemical properties, J. Phys. Chem. Solids 127 (2019) 127–139.
[31] M.R. Anil Kumar, Buzuayehu Abebe, H.P. Nagaswarupa, H.C. Ananda Murthy, C.R. Ravikumar, Fedlu Kedir Sabir, Enhanced photocatalytic and electrochemical performance of TiO_2-Fe_2O_3 nanocomposite: Its applications in dye decolorization and as supercapacitors, Sci. Rep. 10 (2020) 1249.
[32] K.M. Girish, S.C. Prashantha, H. Nagabhushana, C.R. Ravikumar, H.P. Nagaswarupa, Naik Ramachandra, H.B. Premakumar, B. Umesh, Multifunctional Zn_2TiO_4:Sm^{3+}nanopowders: excellent performance as electrochemical sensor and UV photocatalyst, J. Sci: Adv Mater Devices 3 (2018) 151–160.
[33] P. Hajra, S. Shyamal, H. Mandal, P. Fageria, S. Pande, C. Bhattacharya, Photocatalytic activity of Bi_2O_3 nanocrystalline semiconductor developed via chemical-bath synthesis, Electrochim. Acta 123 (2014) 494–500.
[34] M.R. Anil Kumar, B. Mahendra, H.P. Nagaswarupa, B.S. Surendra, C.R. Ravikumar, Krushitha Shetty, "Photocatalytic studies of MgO Nano powder; synthesized by green mediated route", Mater. Today Proc. 5 (2018) 22221–22228.
[35] L. Renuka, K.S. Anantharaju, Y.S. Vidya, H.P. Nagaswarupa, S.C. Prashantha, S.C. Sharma, H. Nagabhushana, G.P. Darshan, A simple combustion method for the synthesis of multi-functional ZrO_2/C_uO nanocomposites: excellent performance as sunlight photocatalysts and enhanced latent fingerprint detection, Appl. Catal. B Environ. 210 (2017) 97–115.
[36] A. Khataee, R.D.C. Soltani, Y. Hanifehpour, M. Safarpour, H.G. Ranijbar, S.W. Joo, Synthesis and characterization of dysprosium-doped ZnO nanoparticles for photocatalysis of a textile dye under visible light irradiation, Ind. Eng. Chem. Res. 53 (2014) 1924–1932.
[37] C.R. Ravikumar, P. Kotteeswaran, V. Bheema Raju, A. Murugan, M.S. Santosh, H.P. Nagaswarupa, S.C. Prashantha, M.R. Anil Kumar, M.S. Shivakumar, Influence of zinc additive and pH on the electrochemical activities of β-nickel hydroxide materials and its applications in secondary batteries, J. Energy Storage 9 (2017) 12–24 Elsevier.
[38] B. Shruthi, B.J. Madhu, V. Bheema Raju, S. Vynatheya, B. Veena Devi, G.V. Jayashree, C.R. Ravikumar, Synthesis, spectroscopic analysis and electrochemical performance of modified β-nickel hydroxide electrode with CuO, J. Sci. Adv Mater. Dev. 2 (2017) 93–98.
[39] C.R. Ravikumar, M.R. Anil Kumar, H.P. Nagaswarupa, S.C. Prashantha, Aarti S. Bhatt, M.S. Santosh, Denis Kuznetsov, CuO embedded β-$Ni(OH)_2$ nanocomposite as advanced electrode materials for supercapacitors, J. Alloys Compd. 738 (2018) 332–339 Elsevier.
[40] H.C. Ananda Murthy, T.D. Zeleke, C.R. Ravikumar, M.R. Anil Kumar, H.P. Nagaswarupa, Electrochemical properties of biogenic silver nanoparticles synthesized using Hagenia abyssinica (brace) JF. Gmel. Medicinal plant leaf extract, Mater. Res. Express 7 (2020), 055016.
[41] N.B. Arun Kumar, J. Sirajudeen, H.P. Nagaswarupa, M.R. Anil Kumar, C.R. Ravikumar, H.C. Ananda Murthy, Electro-chemical and photocatalytic properties of green nickel oxide nanomaterial synthesized using *Plectranthus amboinicus* plant leaf extract, Adv. Mater. Lett. 11 (2020) 20091559.
[42] R. Ranjitha, Aarti S. Bhatt, C.R. Ravikumar, M.S. Santosh, B.K. Jayanna, H.P. Nagaswarupa, K. Sakai, H. Madhyastha, Electroactive Li incorporated cobalt oxide nanostructures for photocatalytic applications, Mater. Res. Express 6 (2019) 1150d6.
[43] C.R. Ravikumar, M.S. Santosh, H.P. Nagaswarupa, S.C. Prashantha, S. Yallappa, M.R. Anil Kumar, Synthesis and characterization of β-$Ni(OH)_2$ embedded with MgO and ZnO nanoparticles as nanohybrids for energy storage devices, Mater. Res. Express 4 (2017) 065503.
[44] M.S. Shivakumar, G. Krishnamurthy, C.R. Ravikumar, Aarti S. Bhatt, Decoration of silver nanoparticles on activated graphite substrate and their electrocatalytic activity for methanol oxidation, J. Sci. Adv Mater. Dev. 4 (2019) 290–298.